Mesoscopic organization of cobalt thin films on clean and oxygen-saturated Fe(001) surfaces

M. Riva,[1] A. Picone,[1,*] D. Giannotti,[1] A. Brambilla,[1] G. Fratesi,[2] G. Bussetti,[1] L. Duò,[1] F. Ciccacci,[1] and M. Finazzi[1]

[1]*Dipartimento di Fisica, Politecnico di Milano, Piazza Leonardo da Vinci 32, 20133 Milano, Italy*

[2]*Dipartimento di Fisica, Università degli Studi di Milano, via Celoria 16, 20133 Milano, Italy*

(Received 6 July 2015; published 21 September 2015)

The different morphologies of Co films grown on either the clean Fe(001) surface and the oxygen-saturated Fe(001)-$p(1 \times 1)$O substrate are investigated by means of scanning tunneling microscopy, Auger electron spectroscopy, and density functional theory. The considered Co coverage range extends beyond the thickness at which layer-by-layer growth is destabilized by plastic deformations induced by the relaxation of the strain accumulated in the film. Our findings indicate that the oxygen overlayer of the Fe(001)-$p(1 \times 1)$O surface floats on top of the growing Co film and strongly influences both the Co nucleation process and the film structural evolution. The layer-dependent islands nucleation of Co films grown on clean Fe(001) substrates, recently associated with a thickness-dependent adatom mobility [A. Picone *et al.*, Phys. Rev. Lett. **113**, 046102 (2014)], is found to be suppressed by the oxygen overlayer. The latter also significantly delays the layer-by-layer instability with respect to the oxygen-free growth. Furthermore, the body-centered-tetragonal/hexagonal-close-packed transition is not observed in the case of Co/Fe(001)-$p(1 \times 1)$O sample, replaced by the development of highly ordered surface undulations. These form a mesoscopic square pattern with the sides aligned to the Fe⟨110⟩ directions, while the surface atomic structure retains the square $p(1 \times 1)$ symmetry in registry with the substrate. Such undulations are likely generated by a highly ordered array of interfacial misfit dislocations running along the Fe⟨110⟩ directions.

DOI: 10.1103/PhysRevB.92.115434 PACS number(s): 68.37.Ef, 81.15.Aa, 68.55.J−

I. INTRODUCTION

The role played by an ordered overlayer of foreign atoms adsorbed on metals or semiconductor surfaces is a widely investigated topic in condensed matter physics and physical chemistry. Theoretical and experimental efforts have highlighted a rich phenomenology of adsorbate-induced effects, such as modifications of the work function [1,2] or surface electronic structure [3,4], enhanced [5–7] or tailored [8–14] surface magnetism, and structural relaxations [15–18], just to name a few. Aside from the above-mentioned phenomena, a widely investigated topic is the so-called surfactant-assisted epitaxial growth [19–24]. In this case, a monolayer (or less) of foreign atoms adsorbed on the substrate before film deposition strongly influences the film morphology, both for heteroepitaxy and homoepitaxy. The surfactant action has been demonstrated to be effective in the following:

(1) Inducing a surface flattening of the growing film [25–28]. This phenomenon has been interpreted either in terms of a surfactant-induced reduction of the difference between the free-energy densities of the film and the substrate [19] or alteration of adatoms diffusion coefficients [20].

(2) Improving heteroepitaxial interfaces, reducing their roughness [29,30] and enhancing their chemical stability [30,31].

(3) Allowing the growth of thin oxide films characterized by a polar termination, otherwise unstable because of the presence of a diverging electrostatic dipole [32,33].

(4) Extending the stability regime of epitaxy-stabilized metastable structures [34–36].

In this paper, we compare the morphology obtained for ultrathin Co films deposited on the clean Fe(001) and on the oxygen-saturated Fe(001)-$p(1 \times 1)$O surfaces. Previous measurements performed with electron-based diffraction and spectroscopic techniques showed that Co, characterized in its bulk form by hexagonal close-packed (hcp) crystal structure at room temperature, can be stabilized in a strained body-centered tetragonal (bct) phase on top of the Fe(001) surface, up to a thickness of about 15 Å [34,37,38]. At larger thickness, a structural transition takes place, turning the metastable bct structure into the thermodynamically stable hcp phase, as evidenced by the development of a $c(2 \times 2)$ low-electron-energy diffraction (LEED) pattern [34].

Furthermore, it was reported that the presence of oxygen on the Fe(001) surface prior to Co deposition can extend the regime of bct stability up to about 30 Å [34,35]. Thicker Co films no longer produced measurable LEED patterns, therefore, the onset of the bct/hcp transition could not be observed, and the mechanisms behind the transition from the ordered to the disordered phase remained unclear. These phenomena are addressed in this paper, where we provide an atomic-scale view of the oxygen surfactant action during the growth of Co thin films on Fe(001) by means of scanning tunneling microscopy (STM).

We adopt the method discussed in Ref. [39] to precisely correlate the STM images with the absolute Co coverage by using wedged samples. This allowed us to directly compare the film morphologies obtained for Co thin films grown on the Fe(001) and on the oxygen-passivated Fe(001)-$p(1 \times 1)$O surface, starting from submonolayer Co films up to the onset of the respective structural transitions. Our measurements reveal that oxygen significantly affects both the nucleation process and the mesoscopic morphological modifications occurring as the thickness approaches the limit at which the bct phase becomes unstable. The evolution of the film's morphology as a function of thickness is interpreted in terms of the energy associated with different atomic distributions at the film surface, as evaluated by calculations based on density functional theory (DFT).

*andrea.picone@polimi.it

II. EXPERIMENT

Samples were prepared in an ultrahigh vacuum (UHV) system (low 10^{-10} mbar pressure range) by starting from a UHV-cleaned MgO(001) single-crystal substrate, over which a 400-nm-thick Fe(001) film was grown by means of molecular beam epitaxy (MBE). Fe(001)-$p(1 \times 1)$O surfaces were obtained by exposing a clean Fe(001) substrate held at 500 °C to 30 L (1 L $= 1.3 \times 10^{-6}$ mbar $\times$ s) of pure O_2 (partial pressure: 2.0×10^{-7} mbar). The samples were then heated at 700 °C for 10 min to remove the excess oxygen from the surface. This procedure generates an oxygen-saturated and well-ordered Fe(001)-$p(1 \times 1)$O superstructure, characterized by one oxygen atom per surface unit cell, lying in the fourfold hollow site of the Fe surface lattice [3].

Co films were grown onto Fe(001) and Fe(001)-$p(1 \times 1)$O substrates by MBE under UHV conditions, with a typical growth rate of about 0.12 equivalent monolayers (ML) per minute,[1] as measured by a quartz microbalance. Wedged films, with Co thickness varying from 0 to 25 ML for Co/Fe(001) samples and from 0 to 47 ML for Co/Fe(001)-$p(1 \times 1)$O samples, were obtained by shadowing the substrate with a movable shutter that was retracted at a constant rate during the growth, as discussed in Ref. [39].

Unless stated otherwise, the substrates were held at room temperature during Co deposition. The sample temperature was measured by a thermocouple mounted in close proximity of the sample position. STM images were acquired by using an Omicron Variable Temperature STM in a UHV chamber connected with the preparation system. STM measurements were acquired at room temperature in constant-current mode with home-made electrochemically etched W tips. After each acquisition of a STM image, the scan area was changed by means of the coarse motion of the piezoelectric drive, following the wedge from highest to lowest coverage. LEED and Auger electron spectroscopy (AES) data were acquired by means of an Omicron SPECTALEED with a retarding field analyzer (total acceptance angle 102°). A 3-kV, 20-μA electron beam was used, with a 3-V peak-to-peak modulation amplitude. A selection of spectra is shown in Fig. 1, which indicates that the intensity of the oxygen-related peaks is unaffected by the presence of the Co film [see spectra (iii) and (iv)], thus indicating that oxygen keeps floating on top of the growing film.

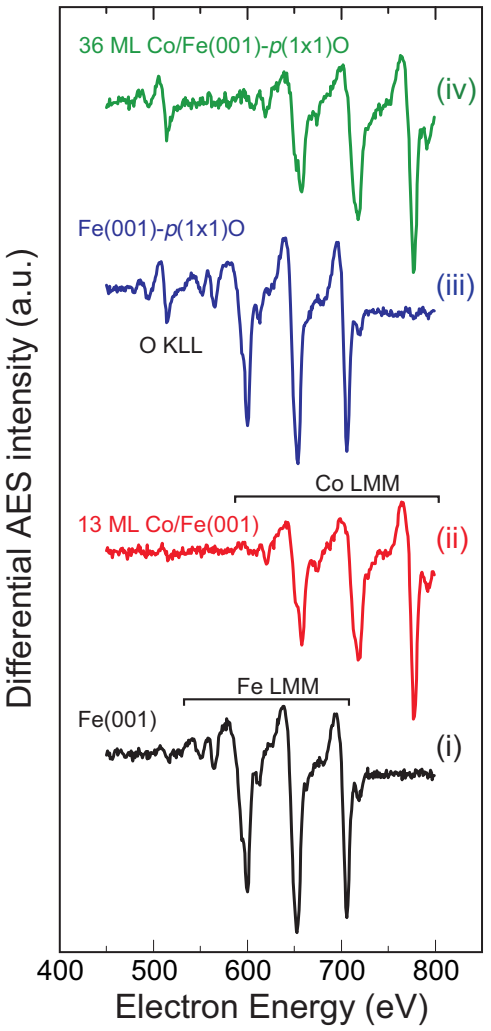

FIG. 1. (Color online) Auger electron spectroscopy data. Spectra (i) and (ii) were acquired before and after deposition of a 13-ML-thick film of Co on the clean Fe(001) surface, respectively. Spectra (iii) and (iv) correspond to the oxygen-saturated Fe(001)-$p(1 \times 1)$O surface and to a 36-ML-thick cobalt film grown on it, respectively. The intensity of the oxygen-related peak remains constant after Co deposition on the Fe(001)-$p(1 \times 1)$O, indicating that the oxygen layer keeps floating on top of the growing film.

III. DFT SIMULATIONS

DFT simulations were performed with ultrasoft pseudopotentials and plane waves as implemented in the QUANTUM ESPRESSO package [40] with the Perdew-Burke-Ernzerhof generalized gradient approximation [41] to the exchange and correlation functional. For Co/Fe(001)-$p(1 \times 1)$O, pseudomorphic Co films were placed on top of a four-layer Fe(001) slab, optimizing all atomic coordinates except the ones of the bottom two Fe layers. In describing Co adatoms, 3×3 surface supercells were adopted with a 5×5 sampling of the surface Brillouin zone. In the direction orthogonal to the slab, the system is separated from its replicas by 11-Å-thick vacuum portions.

The adsorption and diffusion of Co adatoms above the Co surface layer were evaluated by placing the adatom in the high-symmetry sites of the underlying Co lattice and optimizing the geometry. The case of Co on nonoxidized Fe(001)was discussed in Ref. [39], the hollow site (H) being favored over the bridge (B) and top (T) ones, as determined by the respective formation energy F, defined as

$$F = \frac{E^{\mathrm{tot}}_{\mathrm{Co/subs}} - E^{\mathrm{tot}}_{\mathrm{subs}} - \mu_{\mathrm{Co}} N_{\mathrm{Co}}}{N_{\mathrm{Co}}}. \quad (1)$$

[1]One equivalent monolayer (1 ML) equals the amount of Co atoms required to completely saturate the adsorption sites on the Fe substrate, i.e., about 12.2×10^{14} atoms/cm^2. The vertical height of 1 ML is 1.433 Å, corresponding to half of a unit cell of body-centered-cubic Fe.

TABLE I. DFT results for the adatom formation energy F above 1 ML Co on Fe(001)-$p(1 \times 1)$O, calculated for all the geometries shown in Fig. 2. Values in eV.

Bridge	Hollow	Top	Hollow'	Above O	Exchange
0.82	1.82	2.68	2.03	3.14	2.07

Here, $E^{\mathrm{tot}}_{\mathrm{Co/subs}}$ is the DFT total energy of the combined system, $E^{\mathrm{tot}}_{\mathrm{subs}}$ that of the substrate (oxidized Fe or Co/Fe film without adatoms), μ_{Co} the chemical potential of Co adatoms (the reference being the bulk metal), and N_{Co} their number. Lower values indicate more stable configurations.

Since oxygen floats on top of the Co film (see Fig. 1), the formation energy of Co adatoms on Co/Fe(001)-$p(1 \times 1)$O is evaluated by assuming that O atoms only occupy the H surface sites, with no O at the Co/Fe interface. The presence of oxygen atoms drastically changes the picture derived for the Co growth on oxygen-free Fe(001), as it can already be seen from the

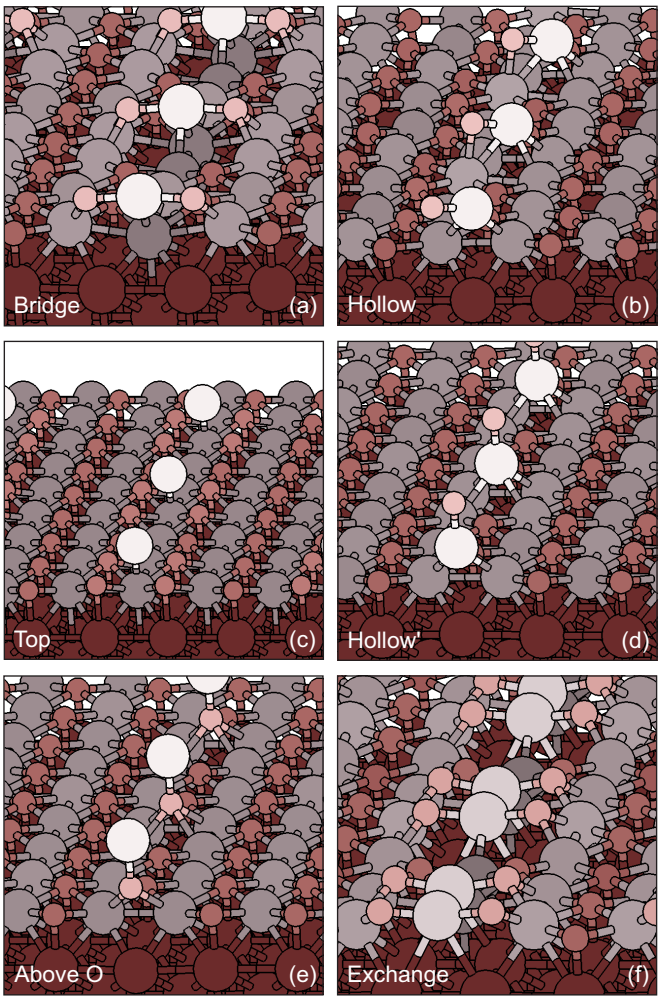

FIG. 2. (Color online) (a)–(e) Different adatom geometries considered for evaluating Co adsorption/diffusion on a 1-ML-thick Co film on Fe(001)-$p(1 \times 1)$O. (f) "Exchange" configuration where two Co atoms (the adatom plus an atom from the surface) lie at the same height above a Co-vacancy site. Small spheres represent O atoms. Different colors indicate atoms at different distances from the Fe layer.

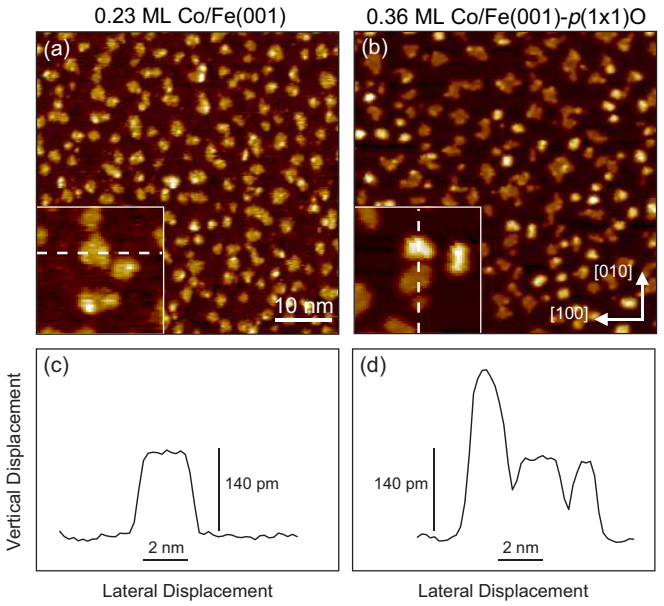

FIG. 3. (Color online) STM constant current topographies for submonolayer deposition of Co on (a) Fe(001) and on (b) the Fe(001)-$p(1 \times 1)$O surface, respectively. Tunneling parameters for images in (a) and (b) are $V_{\mathrm{b}} = 1.6$ V, $I_{\mathrm{t}} = 1$ nA and $V_{\mathrm{b}} = 1.5$ V, $I_{\mathrm{t}} = 1$ nA, respectively. (c), (d) Topographic height measured along the dashed lines of the insets inside panels (a) and (b), respectively.

F values referring to Co adatoms on 1-ML-thick Co films on Fe(001)-$p(1 \times 1)$O reported in Table I. We now find that, among the considered adatom geometries (see Fig. 2), the one characterized by the lowest F value corresponds to Co atoms occupying B sites [Fig. 2(a)], being located between Co and O lattices, while Co occupying a H site [Fig. 2(b)] corresponds to a less favorable situation, 1 eV higher in energy.

On the basis of the results in Table I, diffusion of Co adatoms can occur between two B sites by hopping through the H site. It is worth noticing that Co diffusion may proceed also through adatom exchange with a surface one. Such a diffusion path is characterized by small displacements in the O lattice. We evaluate the energetic cost of this exchange process by considering a symmetric "exchange" (X) configuration where two Co atoms (the adatom plus an atom from the surface) lie at the same height above a Co-vacancy site [see Fig. 2(f)]. We obtain $F = 2.07$ eV, a value slightly larger but still comparable with that of a Co adatom occupying the H site.[2]

IV. RESULTS AND DISCUSSION

A. Submonolayer coverage

Figure 3 compares the experimental morphology resulting from submonolayer deposition of Co on the bare Fe(001) and on the oxygen-saturated Fe(001)-$p(1 \times 1)$O surface. In

[2]The exchange process was not discussed in Ref. [39] for Co diffusion on Co/Fe(001). Actually, when there is no oxygen at the surface of the Co film, this mechanism is associated with a much higher barrier energy than the one characterizing H-B-H hopping ($F_{\mathrm{X}} - F_{\mathrm{H}} = 1.46$ eV vs $E_b = F_{\mathrm{B}} - F_{\mathrm{H}} = 0.88$ eV for 1-ML-thick films).

the former case, the Co coverage is about 0.23 ML, the island density being 8.93×10^{-2} nm^{-2}. In the latter, we measure a higher total coverage of 0.37 ML, yet with a lower island density of 6.05×10^{-2} nm^{-2}. Interestingly, while all islands covering the oxygen-free Fe(001) substrate are one atomic layer high, a non-negligible fraction of the islands growing on Fe(001)-$p(1 \times 1)$O is two layers thick. For the sample reported in Fig. 3(b), about 30% and 3% of the substrate surface is covered by one-layer- and two-layer-thick islands, respectively. The tendency to form two-layer-thick islands was previously reported for Ni growth on Fe(001)-$p(1 \times 1)$O, probably related to a lower oxygen affinity of Ni with respect to the Fe substrate [42]. In that case, however, almost all the Ni islands growing on Fe(001)-$p(1 \times 1)$O were two layers thick. DFT simulations provide a formation energy difference $F_{1\,\mathrm{ML\,Co}} - F_{2\,\mathrm{ML\,Co}} = 0.22$ eV, indicating that two-layer-thick islands should be energetically favored with respect to monolayer ones. The stabilization is, however, somewhat smaller than for Ni/Fe(001)-$p(1 \times 1)$O, for which $F_{1\,\mathrm{ML\,Ni}} - F_{2\,\mathrm{ML\,Ni}} = 0.28$ eV.

In order to verify that the thermodynamically most stable configuration corresponds to two-layer-thick islands, we also performed Co depositions at higher substrate temperatures (not shown). We find that increasing the temperature can indeed promote double-layer Co nucleation. For a 0.42-ML-thick Co film grown on the Fe(001)-$p(1 \times 1)$O substrate held at 100 °C, we observe that the fraction of surface covered by two-layer-thick islands is increased to 6%, while 30% of the surface is covered by single-layer islands. At temperatures higher than 100 °C we observe Co diffusion into the substrate and the number of two-layer-thick islands drastically drops.

B. Layer-by-layer growth and islands nucleation

Figure 4 provides an overview of the growth behavior of the Co thin film on oxygen-free Fe(001) and on Fe(001)-$p(1 \times 1)$O, as determined from the analysis of constant current STM images. As pointed out in our recent work [39], the Co

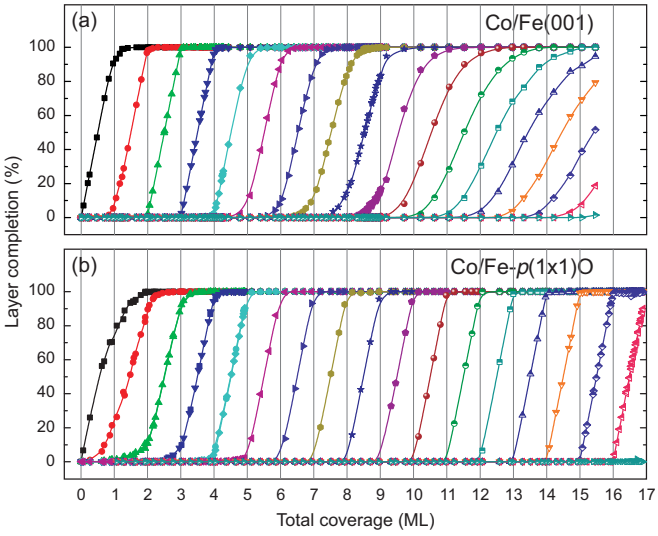

FIG. 4. (Color online) Layer completion as a function of the total Co coverage on (a) oxygen-free Fe(001) and on (b) Fe(001)-$p(1 \times 1)$O.

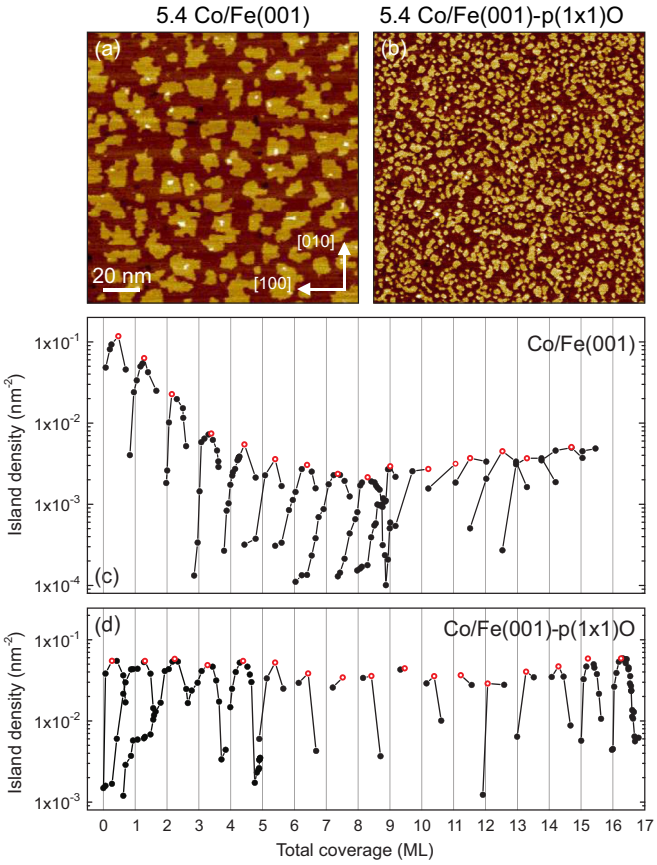

FIG. 5. (Color online) (a) STM topographic image of a 5.4-ML-thick Co film grown on the oxygen-free Fe(001) surface. The island density is 3.60×10^{-3} nm^{-2}. (b) STM topographic image of a 5.4-ML-thick Co film grown on the oxygen-passivated Fe(001)-$p(1 \times 1)$O surface. The island density is 5.25×10^{-2} nm^{-2}. (c), (d) Co island density as a function of the total coverage for Co films grown on (c) oxygen-free Fe(001) and on (d) Fe(001)-$p(1 \times 1)$O, respectively. The local maxima (hollow red dots) correspond to the saturation island density for a given layer.

growth on the oxygen-free surface proceeds in a layer-by-layer mode up to about 9 ML, showing a transition to multilayer growth for higher coverages. At a coverage of 15 ML, four atomic layers are partially completed, corresponding to five surface layers exposed. The Co growth mode on the Fe(001)-$p(1 \times 1)$O surface is remarkably different. After a wetting layer is completed at a coverage equal to 2 ML, a nearly perfect layer-by-layer growth is initiated extending (up to 17 ML) considerably beyond the limit found for Co grown on the oxygen-free surface.

Figure 5 displays the layer-dependent saturation island density, defined as the maximum number of islands per unit area reached between two integer subsequent coverages. Striking differences can be observed for Co growth on the two different substrates. In the case of deposition onto oxygen-free Fe(001), the saturation island density follows a decreasing trend, starting from a value of 1.17×10^{-1} nm^{-2} for the nucleated cobalt islands on the bare Fe(001)substrate, down to 2×10^{-3} nm^{-2} for eight-layer islands (corresponding to Co adatom diffusion on the seventh layer). Conversely, when Co

TABLE II. DFT results for the diffusion of Co adatoms over Co films deposited on Fe(001)-$p(1 \times 1)$O ($E_{HB} = F_H - F_B$; $E_{XB} = F_X - F_B$) compared with the values of the diffusion barrier E_b reported in Ref. [39] for Co/Fe(001). Values in eV.

	Co/Fe(001)-$p(1 \times 1)$O		Co/Fe(001) [39]
Coverage	E_{HB}	E_{XB}	E_b
1 ML	1.00	1.25	0.88
2 ML	0.99	1.08	0.85
3 ML	1.11	0.93	0.55
4 ML	1.16	0.79	0.12
5 ML	1.14	0.71	0.00

is evaporated onto Fe(001)-$p(1 \times 1)$O, the saturation island density is not affected by the Co film thickness, keeping a constant value of about 5×10^{-2} nm^{-2} across the 0–17 ML coverage range.

In the framework of the classical nucleation theory, the island density is related to the diffusion rate of adatoms over the surface [43–45]. Accordingly, the different evolution of islands density in the two systems could be due to a different evolution of the respective diffusion coefficients. To better understand the trends shown in Figs. 5(c) and 5(d), we evaluated the B-H-B hopping barrier E_{HB} as the difference between the H and B formation energies calculated by DFT for a Co coverage ranging from 1 to 5 ML. Additionally, we estimated the activation barrier for Co-Co exchange E_{XB} by comparing the formation energies associated with the X and B geometries. The results are reported in Table II, which also displays the hopping barrier E_b for the nonoxidized surface, from Ref. [39].

Two clearly different trends are obtained for the oxidized and oxygen-free substrates. In case of adatom diffusion on the surface of Co films on oxygen-free Fe(001), the value of E_b decreases quickly as the coverage increases, a phenomenon that was associated with a softening of the Co film as the thickness approaches the limit at which the structural bct-hcp transition occurs [39]. Such a decrease in E_b stems from the stabilization of adatom adsorption on the B site with respect to the H site: having a lower symmetry, the former is affected by larger structural deformations than the latter and is more favored by the thickness-dependent softening [39].

The different topology of the Fe(001)-$p(1 \times 1)$O surface makes B a more stable configuration with respect to H. Consequently, an opposite trend with respect to Co/Fe(001) is observed for the hopping barrier E_{HB}, which slowly increases with the number of Co layers. Actually, the situation is made even more complex by the presence of the additional diffusion channel involving the Co-Co exchange mechanism. The latter is less favorable than B-H-B hopping at low Co coverages, but becomes increasingly convenient as the Co film thickens. We can thus expect both processes to contribute to Co adatom diffusion, possibly with different relative weights as a function of the Co coverage. Eventually, DFT calculations seem to be in good agreement with the observed dramatically different trends shown in Figs. 5(c) and 5(d) since they predict a diffusion barrier for Co/Fe(001)-$p(1 \times 1)$O which does not decrease as rapidly with increasing Co coverage as for Co/Fe(001).

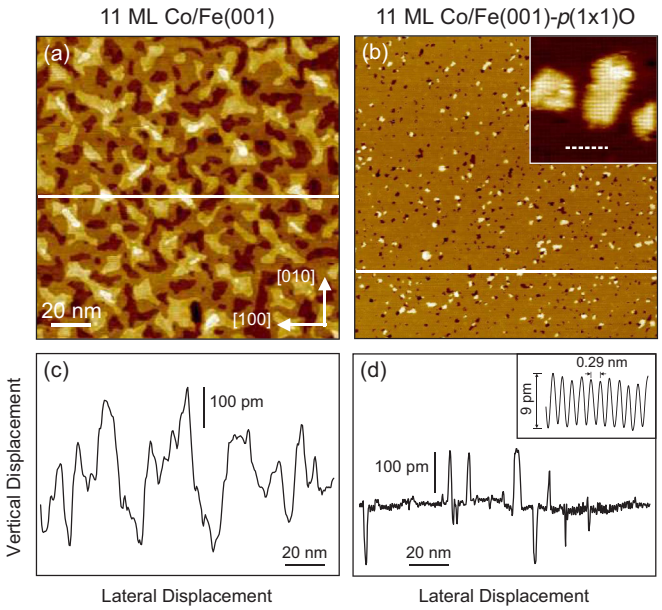

FIG. 6. (Color online) Surface morphologies of 11 ML of Co deposited on (a) the oxygen-free Fe(001) surface and on (b) the Fe(001)-$p(1 \times 1)$O substrate, as evaluated from STM constant current images. The topographic heights corresponding to the continuous white lines in (a) and (b) are displayed in (c) and (d), respectively. The inset in panel (b) shows an atomically resolved STM image acquired in a region straddling a terrace and some Co islands. The measured atomic corrugation, corresponding to the dashed white line, is shown in the inset of panel (d). Tunneling parameters are $V_b = 1$ V, $I_t = 500$ pA for images in (a) and (b). Tunneling parameters for the atomically resolved image in the inset of panel (b) are $V_b = 0.1$ V, $I_t = 5$ nA.

C. Destabilization of the bct phase

Figure 6 compares the surface morphology of 11-ML-thick Co films, a thickness that is slightly above the threshold of the bct to hcp transition for Co grown on oxygen-free Fe(001) [34]. At such thickness, Co films grown on the oxygen-free Fe(001) substrate feature a multilayer morphology, as testified by Fig. 6(c). In addition, it is possible to notice that Co atoms form mounds which are elongated along the ⟨110⟩ in-plane crystallographic directions, similar to those observed in the martensitic transition of Ni films grown on Fe(001) [46,47]. On the other hand, at the same coverage, the topography of the Co film grown on the oxygen-saturated surface is atomically flat, with basically only one exposed layer, as shown in Fig. 6(d). Atomically resolved images acquired over a region straddling a terrace and an island [see inset of Fig. 6(b)] show that both the islands and the terrace are highly ordered and characterized by a square symmetry. In both cases, the atomic corrugation measured in constant current images is about 9 pm, with a periodicity along the [100] direction of approximately 2.9 Å [see inset of Fig. 6(d)], nicely corresponding to the lattice constant of the Fe(001) surface ($a_{Fe} = 2.866$ Å). This measurement in particular confirms that the oxygen atoms arrange in a highly ordered and compact overlayer, completely saturating the surface.

Figure 7 focuses on the morphology of a 15-ML-thick Co film grown on the oxygen-free Fe(001) substrate, i.e., for

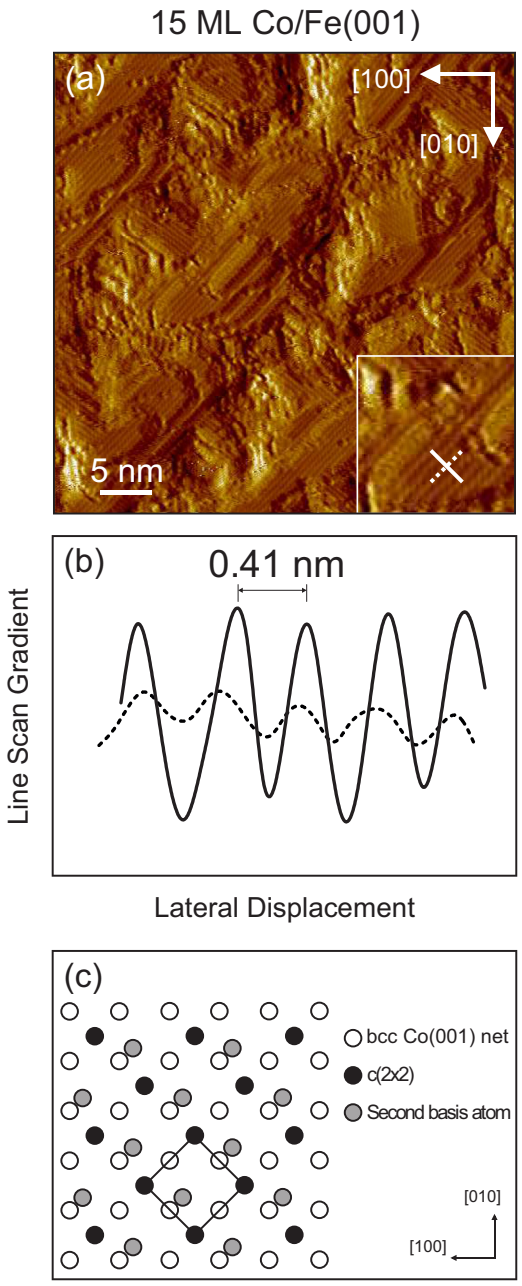

FIG. 7. (Color online) (a) Gradient of the STM topography acquired on a 15-ML-thick Co film grown on the oxygen-free Fe(001) substrate. Tunneling parameters are $V_b = 0.5$ V, $I_t = 400$ pA. (b) Line scans corresponding to the continuous and dashed lines. The corrugation gradient measured along the [110] direction (dashed line) is weaker than that measured along the orthogonal direction (continuous line). (c) Model proposed for the topmost layer of hcp cobalt [34,48]. The compressed square net is rotated by 45° with respect to the [001] substrate direction.

a coverage at which Kim *et al.* reported the presence of a well-developed $c(2 \times 2)$ LEED pattern [34]. In Fig. 7(a), we show the gradient of the constant current STM image in order to evidence the atomic-scale topographic structures, otherwise overwhelmed by the mesoscopic surface topography. Figure 7(b) reports the line scans corresponding to the continuous and dashed lines of the inset of Fig. 7(a). In both cases,

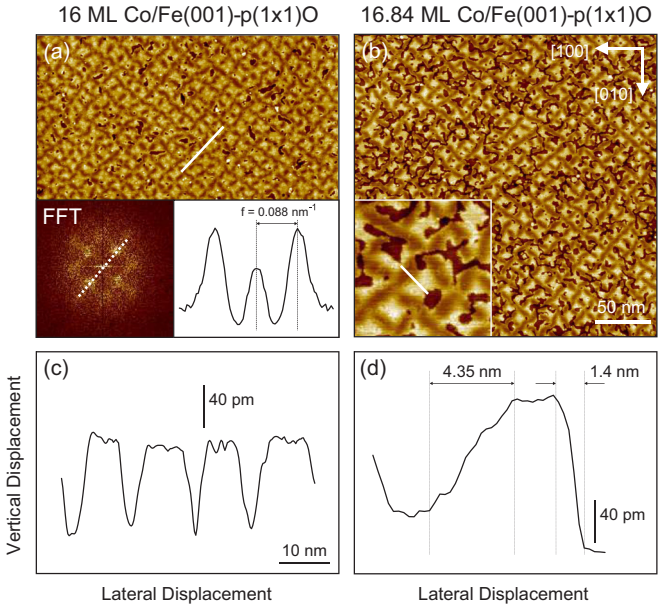

FIG. 8. (Color online) (a) Large-scale STM image of a 16-ML-thick Co film grown on the Fe(001)-$p(1 \times 1)$O surface. The inset on the left shows the FFT of the STM image, from which a periodicity of 11.36 nm can be measured (see in the inset on the right the profile traced along the dashed white line). (b) Large-scale STM image of a 16.84-ML-thick Co film grown on the Fe(001)-$p(1 \times 1)$O surface, with an enlarged view displayed in the inset. (c), (d) STM profiles measured along the lines traced in (a) and (b), respectively. Tunneling parameters for the images in (a) and (b) are $V_b = 1$ V, $I_t = 1$ nA and $V_b = 1$ V, $I_t = 800$ pA, respectively.

the corrugation periodicity is about 0.41 nm, corresponding to the Fe(001) lattice periodicity along the [110] direction $\sqrt{2} \times a_{Fe} = 4.053$ Å. Interestingly, the corrugation intensity measured along the [110] direction is different from that measured along the $[1\bar{1}0]$ direction. Two orthogonal domains are visible in the image. To understand this STM image, we recall the model proposed by Kim *et al.* [34], who report the Co bct to hcp transition as inferred from the development of a $c(2 \times 2)$ LEED pattern. The latter was interpreted as due to hcp Co exposing the $(11\bar{2}0)$ face, with the $(11\bar{2}0)$ rectangular net compressed and rotated by 45° with respect to the in-plane $\langle 001 \rangle$ directions of the substrate [see Fig. 7(c)]. The basis of the compressed rectangular lattice is composed by two atoms. We suggest that the two orthogonal domains visible in Fig. 7(a) depend on the different disposition of the rectangular hcp $(11\bar{2}0)$ net with respect to the square surface lattice, i.e., with the long side aligned along either the [110] or the $[1\bar{1}0]$ direction.

Figure 8(a) displays the sample morphology of a 16-ML-thick Co film grown on the Fe(001)-$p(1 \times 1)$O surface, which is not atomically flat due to the presence of periodic surface undulations, arranged in a square pattern rotated by 45° with respect to the $\langle 110 \rangle$ directions of the substrate.[3] This superstructure is characterized by a periodicity of about 11.36 nm,

[3]The periodic surface undulations start to appear as faint features in STM images corresponding to 14-ML-thick Co films grown on Fe(001)-$p(1 \times 1)$O.

as can be inferred from the fast Fourier transform (FFT) of the STM image [see inset of Fig. 8(a)]. Figure 8(c) displays a line scan corresponding to the sample of Fig. 8(a), showing that at this coverage the undulations are about 80 pm high. Surface undulations are present also for fractional coverages, where monoatomic steps are also visible, as demonstrated by the topographic image shown in Fig. 8(b), corresponding to a Co coverage of 16.84 ML. Figure 8(d) shows a line scan acquired in a region straddling a surface undulation and an atomic step. This image allows one to directly compare the slope measured across a monoatomic Co step and across the undulation. The sharpness of the line scan across the monoatomic step is limited by tip/step convolution effects, resulting in a measured lateral width of 1.4 nm. Conversely, the profile slope is less steep across the surface undulation, with a lateral width of 4.35 nm.

A different mesoscopic pattern, still arranged according with a square lattice rotated by 45° with respect to the ⟨110⟩ directions of the substrate, is visible in the surface topography of a 18-ML-thick Co film grown on Fe(001)-$p(1 \times 1)$O [see Fig. 9(a)]. Within the experimental uncertainty, the superlattice parameter is the same as the one measured for the 16-ML-thick film. In the inset of Fig. 9(a), a blowup is presented, where atomic resolution allows one to detect a square lattice in registry with the substrate, superposed on a conspicuous continuous surface distortion. The topographical elevation of such a distortion appears to be larger than the one observed on the 16-ML-thick sample, as testified by the line scan reaching a corrugation of about 200 pm, as shown in Fig. 9(b). At a Co coverage higher than 18 ML, the roughness associated with the surface distortion further increases, in agreement with the disordered phase reported in Ref. [34]. However, we were able to acquire atomically resolved images (not shown) also in these samples, still observing a square lattice.

In order to explain the development of the mesoscopic square superlattice observed in Co films grown on Fe(001)-$p(1 \times 1)$O from about 14 ML on, we recall that wavelike surface modulations have been related to the development of buried misfit dislocations [49–52]. The dislocation network is often observed to develop at correspondence with the coincidence-site lattice (CSL) between the overlayer and the substrate [53,54]. The CSL is defined as the smallest lattice which is common to the two primitive ones [53,55]. Apparently, the dislocation lines in Co/Fe(001)-$p(1 \times 1)$O remain entirely confined within the film. A possible explanation could be that intercepting the surface would be energetically unfavorable because the strong O-Co covalent bonds would have to be broken and rearranged.

Figure 9(c) displays a geometrical model that can be applied for the interpretation of the surface deformation network in terms of misfit dislocations. The diagram represents the superposition of two square lattices (black continuous lines and red dashed lines) where the lattice misfit is intentionally exaggerated to highlight the coincidence points. Depending on the position of the overlayer lattice sites with respect to the substrate lattice, different coincidence lattices can be formed. In Fig. 9(c), the coincidence points corresponding to top, bridge, and hollow epitaxial sites are marked with circles, triangles, and squares, respectively. The CSL corresponding to top and hollow sites are aligned with the two primitive lattices. Their periodicity Λ is given by $\Lambda = a_o/|f|$, with

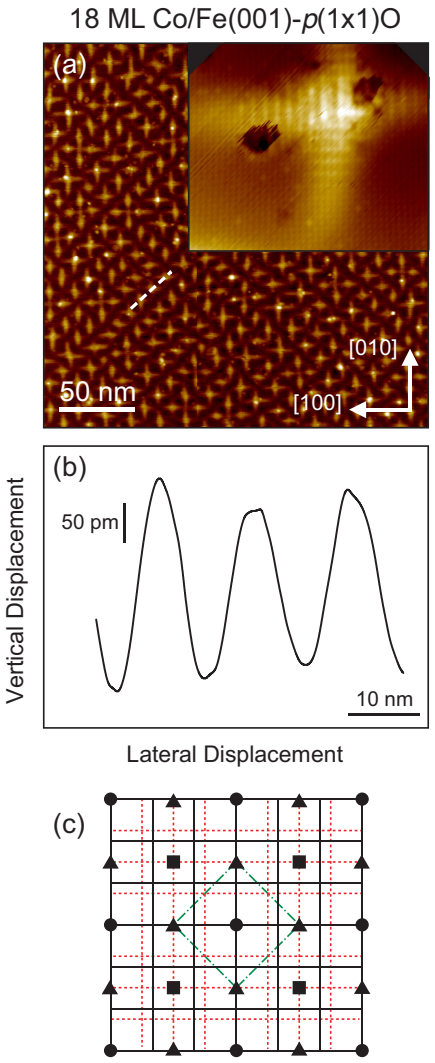

FIG. 9. (Color online) (a) Large-scale STM image of an 18-ML-thick Co film grown on the Fe(001)-$p(1 \times 1)$O surface. Inset: atomically resolved image of the distorted surface. (b) STM profile measured along the line traced in (a). Tunneling parameters are $V_b = 1$ V, $I_t = 500$ pA. (c) Superposition of two square lattices (continuous black lines and dashed red lines) with a lattice mismatch $|f| = 0.75$. The coincidence points corresponding to epilayer atoms placed on the hollow, top, and bridge epitaxial sites are shown as squares, circles, and triangles, respectively. The dashed-dotted green line represents the unit cell of the CSL corresponding to bridge epitaxial sites.

$f = (a_o - a_s)/a_s$, where a_o and a_s are the lattice constants of the overlayer and the substrate, respectively. Indeed, on the other hand, the CSL corresponding to the bridge epitaxial sites is rotated by 45° with respect to the primitive lattices, with a lattice parameter smaller by a factor $\sqrt{2}$. Since our experimental results (Figs. 8 and 9) show that the mesoscopic square network is rotated by 45° with respect to the square net of the substrate, the coincidence lattice to be considered is that formed by the bridge sites. Moreover, the measured periodicity along the [110] direction (11.36 nm) is in good agreement with the CSL that would be obtained by considering the bridge coincidence points. Indeed, the hypothetical bulk phase of

body-centered-cubic (bcc) Co would possess a lattice constant $a_{\mathrm{Co_{bcc}}} = 2.819$ Å [56], yielding a mismatch $|f| = 0.016$ with respect to the Fe(001) lattice ($a_{\mathrm{Fe}} = 2.866$ Å), leading to $\Lambda = a_{\mathrm{Co_{bcc}}}/(\sqrt{2} \times |f|) = 12.45$ nm.

Different crystal structures for the Co films are unlikely. A possible film transition involving the development of face-centered-cubic (fcc) phase (squared primitive unit mesh with a lattice constant $a_{\mathrm{Co_{fcc}}} = 2.506$ Å) [57] would lead to a superstructure periodicity $\Lambda = a_{\mathrm{Co_{fcc}}}/(\sqrt{2} \times |f_{\mathrm{fcc}}|) = 1.99$ nm, by far too small with respect to the one we measure. On the other hand, a transition to the hcp film structure would instead produce CLS without square symmetry since the matching of the Co(11$\bar{2}$0) rectangular net onto the bcc Fe(001) lattice requires 6.64% compression on the long side and a 0.40% compression on the short side. We thus suggest that Co films deposited onto Fe(001)-$p(1 \times 1)$O remain in the bct phase for a layer thickness up to 18 ML and that tensile strain is then relaxed by the insertion of edge-type dislocations running along the Fe⟨110⟩ in-plane directions.

V. CONCLUSIONS

Our data show that the presence of a single layer of oxygen at the surface of Co films growing on Fe(001)-$p(1 \times 1)$O substrates drastically affects both the island nucleation process and the mesoscopic surface morphology as the film thickness is increased from submonolayer coverage up to the limit at which the bct phase becomes unstable.

First, oxygen tends to favor the nucleation of two-layer-thick Co islands before a wetting layer is completed. Second, in the 2–9 ML coverage range, the growth proceeds in an almost perfect layer-by-layer mode for films grown on both the oxygen-free Fe(001) and on the Fe(001)-$p(1 \times 1)$O substrates. However, the layer-dependent island nucleation, characteristic of the Co/Fe(001) system [39], is found to be suppressed by the presence of the oxygen overlayer. Third, at coverages above 9 ML, the well-known bct/hcp structural transition occurring for Co grown on oxygen-free Fe(001) is accompanied by a surface morphological evolution, characterized by the development of mesoscopic mounds elongated along the in-plane ⟨110⟩ crystallographic substrate directions. Conversely, Co films grown on the Fe(001)-$p(1 \times 1)$O surface are atomically flat up to 14 ML, displaying a square symmetry. The surface of Co films thicker than 14 ML is characterized by the development of a pattern of highly ordered undulations, most likely generated by the presence of a square dislocation network, with dislocation lines running along the in-plane Fe⟨110⟩ directions.

We suggest that the atomically flat bct Co films stabilized on the Fe(001)-$p(1 \times 1)$O surface could be an ideal substrate for the growth of high-quality rocksalt structured mono-oxides [58–61], while thicker films could represent an interesting benchmark for the study of the strain relaxation mechanisms driving the destabilization of the Co metastable bct phase [62].

ACKNOWLEDGMENTS

We acknowledge the CINECA Award No. HP10CESYLM, 2014, for the availability of high performance computing resources and support. This work was partially supported by the Italian Ministry of University and Research through the FIRB Project No. RBAP115AYN.

[1] H. W. Hugosson, W. Cao, S. Seetharaman, and A. Delin, J. Phys. Chem. C **117**, 6161 (2013).
[2] A. Michaelides, P. Hu, M.-H. Lee, A. Alavi, and D. A. King, Phys. Rev. Lett. **90**, 246103 (2003).
[3] F. Donati, P. Sessi, S. Achilli, A. Li Bassi, M. Passoni, C. S. Casari, C. E. Bottani, A. Brambilla, A. Picone, M. Finazzi, L. Duò, M. I. Trioni, and F. Ciccacci, Phys. Rev. B **79**, 195430 (2009).
[4] A. Picone, G. Fratesi, A. Brambilla, P. Sessi, F. Donati, S. Achilli, L. Maini, M. I. Trioni, C. S. Casari, M. Passoni, A. Li Bassi, M. Finazzi, L. Duò, and F. Ciccacci, Phys. Rev. B **81**, 115450 (2010).
[5] A. Tange, C. Gao, W. Wulfhekel, and J. Kirschner, Phys. Rev. B **81**, 220404 (2010).
[6] R. Bertacco and F. Ciccacci, Phys. Rev. B **59**, 4207 (1999).
[7] A. Tange, C. L. Gao, B. Y. Yavorsky, I. V. Maznichenko, C. Etz, A. Ernst, W. Hergert, I. Mertig, W. Wulfhekel, and J. Kirschner, Phys. Rev. B **81**, 195410 (2010).
[8] F. Bisio, R. Moroni, M. Canepa, L. Mattera, R. Bertacco, and F. Ciccacci, Phys. Rev. Lett. **83**, 4868 (1999).
[9] J. Hong, R. Q. Wu, J. Lindner, E. Kosubek, and K. Baberschke, Phys. Rev. Lett. **92**, 147202 (2004).
[10] D. Klar, B. Brena, H. C. Herper, S. Bhandary, C. Weis, B. Krumme, C. Schmitz-Antoniak, B. Sanyal, O. Eriksson, and H. Wende, Phys. Rev. B **88**, 224424 (2013).
[11] F. Máca, J. Kudrnovský, V. Drchal, and J. Redinger, Phys. Rev. B **88**, 045423 (2013).
[12] W. Feng, H. L. Meyerheim, K. Mohseni, O. Brovko, V. S. Stepanyuk, N. Jedrecy, R. Felici, and J. Kirschner, Phys. Rev. Lett. **110**, 235503 (2013).
[13] C. Thiede, C. Langenkämper, K. Shirai, A. B. Schmidt, T. Okuda, and M. Donath, Phys. Rev. Applied **1**, 054003 (2014).
[14] G. Berti, A. Brambilla, A. Calloni, G. Bussetti, M. Finazzi, L. Duò, and F. Ciccacci, Appl. Phys. Lett. **106**, 162408 (2015).
[15] S. R. Chubb and W. E. Pickett, Phys. Rev. Lett. **58**, 1248 (1987).
[16] A. Eichler and J. Hafner, Phys. Rev. B **62**, 5163 (2000).
[17] S. S. Parihar, H. L. Meyerheim, K. Mohseni, S. Ostanin, A. Ernst, N. Jedrecy, R. Felici, and J. Kirschner, Phys. Rev. B **81**, 075428 (2010).
[18] V. C. Schwindt, J. Ardenghi, P. Bechthold, E. Gonzàlez, P. Jasen, A. Juan, B. Batic, and M. Jenko, Appl. Surf. Sci. **315**, 252 (2014).
[19] M. Copel, M. C. Reuter, E. Kaxiras, and R. M. Tromp, Phys. Rev. Lett. **63**, 632 (1989).
[20] J. Camarero, J. Ferrón, V. Cros, L. Gómez, A. L. Vázquez de Parga, J. M. Gallego, J. E. Prieto, J. J. de Miguel, and R. Miranda, Phys. Rev. Lett. **81**, 850 (1998).
[21] H. L. Meyerheim, D. Sander, R. Popescu, W. Pan, I. Popa, and J. Kirschner, Phys. Rev. Lett. **99**, 116101 (2007).
[22] K.-J. Hsueh, C.-J. Tsai, S.-Y. Wu, H.-L. Chou, F. Bisio, C.-C. Kuo, and W.-C. Lin, J. Appl. Phys. **114**, 203907 (2013).

[23] C.-J. Tsai, K.-J. Hsueh, N. Plusnin, C.-C. Kuo, and W.-C. Lin, Appl. Surf. Sci. **313**, 166 (2014).

[24] Z.-j. Wang, A. Dong, M. Wei, Q. Fu, and X. Bao, Appl. Phys. Lett. **104**, 181604 (2014).

[25] A. Picone, A. Brambilla, A. Calloni, L. Duò, M. Finazzi, and F. Ciccacci, Phys. Rev. B **83**, 235402 (2011).

[26] A. Calloni, A. Picone, A. Brambilla, M. Finazzi, L. Duò, and F. Ciccacci, Surf. Sci. **605**, 2092 (2011).

[27] H. Fukumoto, M. Miyazaki, Y. Aoki, K. Nakatsuji, and H. Hirayama, Surf. Sci. **611**, 49 (2013).

[28] T. Kojima, M. Mizuguchi, and K. Takanashi, Surf. Sci. **619**, 44 (2014).

[29] S. Amir, M. Gupta, A. Gupta, and J. Stahn, Appl. Phys. A **111**, 495 (2013).

[30] S. M. Amir, M. Gupta, S. Potdar, A. Gupta, and J. Stahn, J. Appl. Phys. **114**, 024307 (2013).

[31] A. Tekiel, J. Topple, Y. Miyahara, and P. Grütter, Nanotechnology **23**, 505602 (2012).

[32] X. Tan and P. Zapol, Phys. Rev. B **86**, 045422 (2012).

[33] V. K. Lazarov, Z. Cai, K. Yoshida, K. H. L. Zhang, M. Weinert, K. S. Ziemer, and P. J. Hasnip, Phys. Rev. Lett. **107**, 056101 (2011).

[34] S. K. Kim, C. Petersen, F. Jona, and P. M. Marcus, Phys. Rev. B **54**, 2184 (1996).

[35] L. Duò, R. Bertacco, G. Isella, F. Ciccacci, and M. Richter, Phys. Rev. B **61**, 15294 (2000).

[36] M. Á. Niño, J. Camarero, L. Gómez, J. Ferrón, J. J. de Miguel, and R. Miranda, J. Phys.: Condens. Matter **20**, 265008 (2008).

[37] G. C. Gazzadi and S. Valeri, Europhys. Lett. **45**, 501 (1999).

[38] H. Li and B. P. Tonner, Phys. Rev. B **40**, 10241 (1989).

[39] A. Picone, M. Riva, G. Fratesi, A. Brambilla, G. Bussetti, M. Finazzi, L. Duò, and F. Ciccacci, Phys. Rev. Lett. **113**, 046102 (2014).

[40] P. Giannozzi, S. Baroni, N. Bonini, M. Calandra, R. Car, C. Cavazzoni, D. Ceresoli, G. L. Chiarotti, M. Cococcioni, I. Dabo, A. D. Corso, S. de Gironcoli, S. Fabris, G. Fratesi, R. Gebauer, U. Gerstmann, C. Gougoussis, A. Kokalj, M. Lazzeri, L. Martin-Samos, N. Marzari, F. Mauri, R. Mazzarello, S. Paolini, A. Pasquarello, L. Paulatto, C. Sbraccia, S. Scandolo, G. Sclauzero, A. P. Seitsonen, A. Smogunov, P. Umari, and R. M. Wentzcovitch, J. Phys.: Condens. Matter **21**, 395502 (2009).

[41] J. P. Perdew, K. Burke, and M. Ernzerhof, Phys. Rev. Lett. **77**, 3865 (1996).

[42] A. Picone, G. Bussetti, M. Riva, A. Calloni, A. Brambilla, L. Duò, F. Ciccacci, and M. Finazzi, Phys. Rev. B **86**, 075465 (2012).

[43] H. Brune, Surf. Sci. Rep. **31**, 125 (1998).

[44] *Islands Mounds and Atoms*, edited by T. Michely and J. Krug (Springer, Berlin, 2004).

[45] M. Einax, W. Dieterich, and P. Maass, Rev. Mod. Phys. **85**, 921 (2013).

[46] G. Bussetti, M. Riva, A. Picone, A. Brambilla, L. Duò, M. Finazzi, and F. Ciccacci, New J. Phys. **14**, 053048 (2012).

[47] G. Bussetti, M. Riva, A. Picone, A. Brambilla, L. Duò, F. Ciccacci, and M. Finazzi, Nanosci. Nanotechnol. Lett. **4**, 1092 (2012).

[48] C. P. Wang, S. C. Wu, F. Jona, and P. M. Marcus, Phys. Rev. B **49**, 17391 (1994).

[49] R. Stalder, H. Sirringhaus, N. Onda, and H. von Känel, Appl. Phys. Lett. **59**, 1960 (1991).

[50] G. Springholz, Appl. Surf. Sci. **112**, 12 (1997).

[51] G. Jnawali, H. Hattab, F.-J. Meyer zu Heringdorf, B. Krenzer, and M. Horn-von Hoegen, Phys. Rev. B **76**, 035337 (2007).

[52] G. Jnawali, H. Hattab, C. Bobisch, A. Bernhart, E. Zubkov, R. Möller, and M. H. von Hoegen, Surf. Sci. **603**, 2057 (2009).

[53] G. Renaud, P. Guénard, and A. Barbier, Phys. Rev. B **58**, 7310 (1998).

[54] P. Torelli, E. Soares, G. Renaud, S. Valeri, X. Guo, and P. Luches, Surf. Sci. **601**, 2651 (2007).

[55] W. Bollmann, *Crystal Defects and Crystalline Interfaces* (Springer, Berlin, 1970).

[56] G. A. Prinz, Phys. Rev. Lett. **54**, 1051 (1985).

[57] J. R. Cerda, P. L. de Andres, A. Cebollada, R. Miranda, E. Navas, P. Schuster, C. M. Schneider, and J. Kirschner, J. Phys.: Condens. Matter **5**, 2055 (1993).

[58] M. Finazzi, L. Duò, and F. Ciccacci, Surf. Sci. Rep. **64**, 139 (2009).

[59] *Magnetic Properties of Antiferromagnetic Oxide Materials: Surfaces, Interfaces and Thin Films*, edited by M. Finazzi, L. Duò, and F. Ciccacci (Wiley, Weinheim, 2010).

[60] M. Riva, A. Picone, G. Bussetti, A. Brambilla, A. Calloni, G. Berti, L. Duò, F. Ciccacci, and M. Finazzi, Surf. Sci. **621**, 55 (2014).

[61] A. Calloni, G. Berti, A. Brambilla, M. Riva, A. Picone, G. Bussetti, M. Finazzi, F. Ciccacci, and L. Duò, J. Phys.: Condens. Matter **26**, 445001 (2014).

[62] O. O. Brovko, D. I. Bazhanov, H. L. Meyerheim, D. Sander, V. S. Stepanyuk, and J. Kirschner, Surf. Sci. Rep. **69**, 159 (2014).